

# Comptonization of Infrared Radiation from Hot Dust by Relativistic Jets in Quasars

M. Błażejowski and M. Sikora

*Nicolaus Copernicus Astronomical Center, Bartycka 18, 00-716 Warsaw, Poland*

blazejow@camk.edu.pl

R. Moderski<sup>1</sup>

*JILA, University of Colorado, Boulder, CO 80309-0440, USA*

and

G. M. Madejski<sup>2</sup>

*Laboratory for High Energy Astrophysics, NASA/GSFC, Greenbelt, MD 20771, USA*

**Accepted for publication in the *Astrophysical Journal*, Dec. 20, 2000 issue**

## ABSTRACT

We demonstrate the importance of near-infrared radiation from hot dust for Compton cooling of electrons/positrons in quasar jets. In our model, we assume that the non-thermal radiation spectra observed in OVV quasars are produced by relativistic electrons/positrons accelerated in thin shells which propagate down the jet with relativistic speeds. We show that the Comptonization of the near-IR flux is likely to dominate the radiative output of OVV quasars in the energy range from tens of keV up to hundreds of MeV, where it exceeds that produced by Comptonization of the UV radiation reprocessed and rescattered in the Broad Emission Line (BEL) region. The main reason for this lies in the fact that the jet encounters the ambient IR radiation over a relatively large distance as compared to the distance where the energy density of the broad emission line light peaks. In the soft - to mid energy X-ray band, the spectral component resulting from Comptonization of the near-IR radiation joins smoothly with the synchrotron-self-Compton component, which may be responsible for the soft X-ray flux. At the highest observed  $\gamma$ -ray energies, in the GeV range, Comptonization of broad emission lines dominates over other components.

*Subject headings:* quasars: jets, radiation mechanisms, pairs, X-rays, gamma-rays

---

<sup>1</sup>also: Nicolaus Copernicus Astronomical Center, Warsaw

<sup>2</sup>also: Dept. of Astronomy, University of Maryland, College Park, MD 20771, USA

## 1. INTRODUCTION

Recent discovery that blazars are strong and variable  $\gamma$ -ray emitters (von Montigny *et al.* 1995) provided independent evidence that the blazar phenomenon (smooth continuum emission in all observable bands; large-amplitude, rapid variability; and high linear polarization) is produced by relativistic sub-psec jets which are oriented at small angles to the line of sight (Doni & Ghisellini 1995; for a recent review, see, *e.g.*, Ulrich, Maraschi, & Urry 1997). Radio loud quasars with such an orientation of the jet are observed as optically-violent-variable (OVV) and highly polarized quasars, while the line-weak radio galaxies are seen as BL Lac objects.

Non-thermal spectra of blazars can be divided into two components, the low energy component, commonly interpreted in terms of the synchrotron radiation mechanism, and the high energy component, presumably produced by the inverse-Compton (IC) process (see, *e.g.*, review by Sikora 1997). In BL Lac objects, the IC energy losses of relativistic electrons/positrons are likely to be dominated by the synchrotron self-Compton (SSC) process (Mastichiadis & Kirk 1997; Ghisellini *et al.* 1998; Coppi & Aharonian 1999), whereas in the OVV quasars, Comptonization of the diffuse ambient radiation field is probably more important (Sikora, Begelman, & Rees 1994 [hereafter: SBR94]; Blandford & Levinson 1995). The above, however, should be regarded as a trend rather than the rule, and, *e.g.*, the case of BL Lacertae shows that Comptonization of external radiation can be important also in BL Lac objects (Madejski *et al.* 1999).

The models proposing that  $\gamma$ -rays in OVV quasars result from Comptonization of the diffuse ambient radiation field are commonly known as external radiation Compton (ERC) models. There are many variants of the ERC models. In some of them, radiation sources are approximated by homogeneous “blobs” propagating along the jet (SBR94; Ghisellini *et al.* 1998; Kusunose, Takahara, & Li 2000), while in others — by an inhomogeneous flow (Blandford & Levinson 1995). They also differ regarding the dominant diffuse ambient radiation field. For small distances,  $< 10^{16-17}$  cm, this can be provided directly by the accretion disc (Dermer & Schlickeiser 1993), while at larger distances, the broad emission lines (BEL) and near-IR radiation from hot dust are likely to dominate (SBR94). In the “blob” model, the distance along the jet where most of the  $\gamma$ -ray flux is produced can be estimated from variability time scale and from the location of the spectral break where the luminosity of the Compton component peaks. The 1  $\div$  3 day time scales of  $\gamma$ -ray outbursts and typical location of their spectral breaks in the 1  $\div$  30 MeV range are consistent with production of  $\gamma$ -rays by Comptonization of light from BEL regions and dust at distances  $10^{17} - 10^{18}$  cm (see Table 1 in SBR94).

The situation in the X-ray band is more complex. In part, the SSC process may be important in the soft/mid energy X-ray bands (Inoue & Takahara 1996; Kubo *et al.* 1998). Furthermore, X-ray variability usually shows lower amplitude than variability in the  $\gamma$ -ray band (Sambruna 1997; Wehrle *et al.* 1998). This suggests that X-rays produced co-spatially with  $\gamma$ -rays are contaminated by another source of X-rays, possibly located at larger distances along the jet and therefore varying on much longer time scales. Superposition of radiation components produced at lower and

higher distances can also explain progressively weaker variability in the synchrotron component at lower frequencies (Brown *et al.* 1989; Edelson 1992; Hartman *et al.* 1996; Ulrich, Maraschi & Urry 1997). Since both sources located at smaller and larger distances are related to dissipation events presumably triggered by collisions between inhomogeneities propagating down the jet at different velocities, one can expect that location and strength of these collisions change with time. As a result, the relative amplitude of different spectral components may also be changing from epoch to epoch. The best studied example is the quasar 3C 279, which is usually very variable in the optical band (this is an OVV quasar), but during the high energy flare in 1996, the optical flux varied less than 20% (Wehrle *et al.* 1998).

As was demonstrated by Sikora & Madejski (2000), studies of X-ray radiation in OVV quasars allow a verification of the presence of low energy electrons in a jet. This, in turn, can be used to estimate the pair content of quasar jets. We conduct such studies in this paper by more detailed modeling of production of radiation. This is also the first work where the contribution of all three Compton components: SSC, C(BEL) and C(IR) is taken into account simultaneously.

This paper is organized as follows: in §2 we describe our model of non-thermal flare production in relativistic jets. In §3 we use the model to reproduce typical spectra observed in  $\gamma$ -ray detected OVV quasars and illustrate their dependence on the low energy break in the electron/positron injection function. We use two classes of models, one where the radiative output is dominated by Comptonization of IR radiation from hot dust, and another where  $\gamma$ -ray flux results from Comptonization of broad emission lines. In that section, we also discuss the model parameters and, in particular, calculate the pair content of the jet plasma, required to provide the observed spectra. We summarize our main conclusions in §4.

## 2. THE MODEL

### 2.1. Evolution of the Electron Energy Distribution

In our model, we assume that relativistic electrons/positrons are enclosed within a very thin shell which propagates along the jet with relativistic speed. With this, we can describe evolution of the electron energy distribution,  $N_\gamma$ , using the following continuity equation (see, *e.g.*, Moderski, Sikora, & Bulik 2000)

$$\frac{\partial N_\gamma}{\partial r} = -\frac{\partial}{\partial \gamma} \left( N_\gamma \frac{d\gamma}{dr} \right) + \frac{Q}{c\beta\Gamma}, \quad (1)$$

where the rate of electron/positron energy losses is

$$\frac{d\gamma}{dr} = \frac{1}{\beta c\Gamma} \left( \frac{d\gamma}{dt'} \right)_{rad} - \frac{2}{3} \frac{\gamma}{r}, \quad (2)$$

$r$  is the distance from the central engine,  $\Gamma$  is the bulk Lorentz factor,  $\beta = \sqrt{\Gamma^2 - 1}/\Gamma$ ,  $\gamma$  is the random Lorentz factor of an electron/positron,  $Q$  is the rate of injection of relativistic elec-

trons/positrons, and  $dr = \beta c \Gamma dt'$ . The second term on the right-hand side of Eq. (2) represents the adiabatic losses for two-dimensional expansion of the jet. Radiative energy losses are dominated by:

(1) synchrotron radiation,

$$\left(\frac{d\gamma}{dt'}\right)_S = -\frac{4\sigma_T}{3m_e c} u'_B \gamma^2, \quad (3)$$

(2) Comptonization of synchrotron radiation,

$$\left(\frac{d\gamma}{dt'}\right)_{SSC} = -\frac{4\sigma_T}{3m_e c} u'_S \gamma^2, \quad (4)$$

and (3) Comptonization of external radiation,

$$\left(\frac{d\gamma}{dt'}\right)_{ERC} = -\frac{16\sigma_T}{9m_e c} (u_{diff(BEL)} + u_{diff(IR)}) \Gamma^2 \gamma^2, \quad (5)$$

where  $u'_B = B'^2/8\pi$  is the magnetic field energy density,  $u'_S$  is the energy density of the synchrotron radiation field,  $u_{diff(BEL)} \simeq \frac{\partial L_{BEL}/\partial \ln r}{4\pi r^2 c}$  is the energy density of the broad emission line field present at the actual distance of a source/shell propagating downstream a jet,  $u_{diff(IR)} \simeq \xi_{IR} 4\sigma_{SB} T^4/c$  is the energy density of the infrared radiation field,  $\xi_{IR}$  is the fraction of the central radiation reprocessed into near infrared by hot dust, and  $T$  is temperature of dust assumed to be located at  $r_{IR} > r$  (see Eq. 17). Note that the expression for  $u_{diff(BEL)}$  does not include the contribution from emission lines produced at much larger or smaller distances than  $r$ . This is because for any smooth radial distribution of external diffuse radiation field, as is likely to be the case of BELR in quasars (Peterson 1993), the lines produced over larger distances ( $> r$ ) provide much lower energy densities, while the lines produced at smaller distances are very significantly redshifted in the shell frame. Here, as elsewhere in the paper, primed quantities denote measurements made in the source co-moving frame. Energy density of the synchrotron radiation is given by:

$$u'_S = \frac{1}{2\pi a^2 c} \int_{\nu'_{abs}}^{\nu'_{S,max}} \nu' L'_{S,\nu'} d \ln \nu' \quad (6)$$

where  $a$  is the cross section radius of the jet at a distance where the outburst is produced,  $\nu'_{abs}$  is the frequency at which the optical thickness due to synchrotron-self-absorption is equal to unity<sup>3</sup>,  $h\nu'_{S,max} = (4/3)\gamma_{max}^2 (B'/B_{cr}) m_e c^2$ ,  $B_{cr} \simeq 4.4 \times 10^{13}$  Gauss, and

$$\nu' L'_{S,\nu'} \simeq \frac{1}{2} (\gamma N_\gamma) m_e c^2 \left| \frac{d\gamma}{dt'} \right|_S. \quad (7)$$

It should be mentioned here that in the case of thin shell geometry, the synchrotron energy density, given by formula (6), is reached throughout the source on much shorter time scale than  $a/c$ , and,

---

<sup>3</sup>We calculate  $\nu'_{abs}$  using an approximate formula given by SBR94 and derived assuming spherical geometry of the source. For the shell geometry,  $\nu'_{abs}$  is larger and angle dependent, but never exceeds the value for spherical case by more than  $\leq (a/\lambda')^{2/7}$ .

therefore, unlike the case of spherical sources, the SSC flares are not expected to lag significantly behind the synchrotron flares. We also note that our assumption about the *comoving* thinness of shells is well justified by the detailed studies of shocks produced by collisions of inhomogeneities moving with different velocities, provided their Lorentz factors differ by less than a factor 2 (see, e.g., Komissarov and Falle 1997).

## 2.2. Modeling of the Radiation Spectra

Since we consider only the contribution to the overall spectra by the regions of the jet which are optically thin, the observed spectra can be computed using the following formula

$$\nu L_\nu(t) \simeq \frac{1}{\Omega_j} \iint_{\Omega_j} \nu' L'_{\nu'}[r; \theta'] \mathcal{D}^4 d \cos \theta d\phi, \quad (8)$$

where

$$r = \frac{c\beta t}{1 - \beta \cos \theta}, \quad (9)$$

$\mathcal{D} = [\Gamma(1 - \beta \cos \theta)]^{-1} \equiv \Gamma(1 + \beta \cos \theta')$  is the Doppler factor,  $\theta$  is the angle between velocity of the shell element and direction to the observer,  $\nu = \mathcal{D}\nu'$ , and  $t$  is the observed time (see Appendix A). The intrinsic synchrotron luminosity,  $\nu' L'_{S, \nu'}$ , is given by Eq. (7). The intrinsic SSC luminosity is (see, e.g., Chiang & Dermer 1999)

$$\nu' L'_{SSC, \nu'} = \frac{\sqrt{3}\sigma_T}{8\Omega_j r^2} \nu'^{3/2} \int_{\nu'_1}^{\nu'_2} N_\gamma \left[ \gamma = \sqrt{\frac{3\nu'}{4\nu'_S}} \right] L'_{S, \nu'} \nu'^{-3/2} d\nu'_S, \quad (10)$$

where

$$\nu'_1 = \text{Max} \left[ \nu'_{abs}; \frac{3\nu'}{4\gamma_{max}^2} \right], \quad (11)$$

and

$$\nu'_2 = \text{Min} \left[ \nu'_{S, max}; \frac{3\nu'}{4\gamma_{min}^2} \right]. \quad (12)$$

In contrast to the synchrotron and SSC emission which is isotropic in the co-moving frame, the radiation produced by Comptonization of external radiation is anisotropic, and thus

$$\nu' L'_{C(i), \nu'}[\theta'] \equiv 4\pi \frac{\partial(\nu' L'_{C(i), \nu'})}{\partial \Omega'_{\vec{n}'_{obs}}} \simeq \frac{1}{2} \gamma N_\gamma m_e c^2 \left. \frac{d\gamma}{dt'} \right|_{C(i)} [\theta'], \quad (13)$$

where

$$\left. \frac{d\gamma}{dt'} \right|_{C(i)} [\theta'] \simeq \frac{4\sigma_T}{3m_e c} \gamma^2 \mathcal{D}^2 u_i, \quad (14)$$

and  $i$ : BEL or IR. The right-hand side of Eq. (13) is calculated for

$$\gamma = \sqrt{\frac{\nu'}{\mathcal{D}\nu_i}} = \frac{1}{\mathcal{D}} \sqrt{\frac{\nu}{\nu_i}}. \quad (15)$$

Anisotropy of the ERC process (Eq. 14) and its astrophysical implications have been extensively discussed by Dermer (1995), and some general comments on the significance of this anisotropy can be found in Sikora (1997).

### 2.3. Application to Homogeneous ERC Models

Using the formalism given above, we consider homogeneous ERC models. Specifically, our goal is to compare two scenarios: in the first case,  $\gamma$ -rays are produced by Comptonization of near-IR radiation (which we subsequently denote as models **A**), while in the second case, it is due to Comptonization of broad emission line photons (hereafter models **B**). Our model assumptions are:

- electron/positron injection function is a power-law,  $Q = K\gamma^{-p}$ , for  $\gamma_b < \gamma < \gamma_{max}$ , and has a low energy tail,  $Q \propto \gamma^{-1}$ , for  $\gamma < \gamma_b$ ;
- $\gamma_b$  is lower than the energy of the break,  $\gamma_c$ , produced due to cooling effect (SBR94<sup>4</sup>) and, therefore, it is the latter which determines the position of luminosity peaks of the spectral components C(BEL) and C(IR);
- electrons/positrons are injected at a constant rate within a distance range  $(r_0; 2r_0)$  and uniformly fill the shell whose radial width is  $\lambda' < r_0/\Gamma$ ;
- the shell propagates down the conical jet with a constant Lorentz factor  $\Gamma$ . The half-opening angle of the jet is  $\theta_j = 1/\Gamma$ ;
- the intensity of the magnetic field is  $B(r) = (r_0/r)B_0$ , the energy density of broad emission lines is  $u_{diff(BEL)} = (r_0/r)^2 u_{BEL,0}$ , and the energy density of infrared radiation is  $u_{IR} = const$ ;
- the observer is located at an angle  $\theta_{obs} = 1/\Gamma$ .

With the above assumptions, the model approximates a situation where the shell containing relativistic plasma is formed due to collision of two perturbances moving down the jet with different velocities (see, *e.g.*, SBR94 and Rees & Mészáros 1994). The low energy break in the electron/positron injection function,  $\gamma_b$ , corresponds to the characteristic energy of pre-heated electrons/positrons (see, *e.g.*, Kirk, Rieger, & Mastichiadis 1998), and the low energy tail below this break is introduced to mimic a limited efficiency of the pre-heating process, nature of which is very uncertain (Hoshino *et al.* 1992; Levinson 1996; McClements *et al.* 1997).

Input parameters of the models were chosen to reproduce typical features of OVV quasar flares: location of the  $\gamma$ -ray luminosity peak in the 1 – 30 MeV range; apparent  $\gamma$ -ray luminosity in the range  $10^{47-48}$  erg s<sup>-1</sup>; apparent synchrotron luminosity in the range  $10^{46-47}$  erg s<sup>-1</sup>; deficiency of radiation in the soft/mid X-ray bands; maximum synchrotron frequency,  $\nu_{S,max} \sim 10^{15}$  Hz; and time scale of  $\gamma$ -ray flares on the order of days. For broadband spectra of blazars see, *e.g.*, von Montigny *et al.* (1995) and Fossati *et al.* (1998); for time scales of rapid (daily)  $\gamma$ -ray variability

---

<sup>4</sup>Note that in SBR94 the cooling energy break is denoted by  $\gamma_b$ , while in our paper, it denotes the low energy break in the injection function.

see, *e.g.*, Michelson *et al.* (1994), Mattox *et al.* (1997) and Wehrle *et al.* (1998).

### 3. RESULTS AND DISCUSSION

As it was shown by SBR94, the high energy  $\gamma$ -rays detected by EGRET on board *CGRO* from OVV quasars can be produced by Comptonization of broad emission line light as well as by Comptonization of infrared radiation (see Table 1 in SBR94). Whereas the broad emission line flux gained a lot of attention as a good candidate for the dominant source of seed photons for the inverse Compton process in a jet, the infrared radiation from dust was largely ignored in the literature (see, however, Wagner *et al.* 1995a and references therein). To the best of our knowledge, this paper is the first where production of *both* spectral components, C(IR) and C(BEL), is treated simultaneously. We discuss the energy density of those components below.

Regarding the diffuse radiation field on sub-parsec scales provided by broad emission line clouds, the line luminosities in radio loud quasars are typically in the range  $10^{44} - 10^{46}$  erg s<sup>-1</sup> (Celotti, Padovani & Ghisellini 1997; Cao & Jiang 1999). Assuming that the scale of the broad emission line region is on the order of the distance at which non-thermal flares are produced in a jet, one can find that the corresponding energy density at a distance  $r = 10^{18} r_{18}$  cm is

$$u_{diff(BEL)} \simeq \frac{L_{BEL}}{4\pi r^2 c} \simeq 3 \times 10^{-3} \frac{L_{BEL,45}}{r_{18}^2} \text{ erg s}^{-1}, \quad (16)$$

where  $L_{BEL,45} = L_{BEL}/10^{45}$  erg s<sup>-1</sup>. For the diffuse IR radiation, just as in the cases of Seyfert galaxies and radio quiet quasars, the spectra of lobe-dominated radio loud quasars show very prominent near-IR bumps (Sanders *et al.* 1989; de Vries *et al.* 1998). These bumps are commonly interpreted as thermal radiation produced by hot dust. Such dust is expected to be heated by UV radiation of an accretion disc and located in the innermost parts of a geometrically thick molecular torus, at a distance

$$r_{IR} \simeq \sqrt{\frac{L_{UV}}{4\pi\sigma_{SB}T^4}} \simeq 4 \times 10^{18} \frac{L_{UV,46}^{1/2}}{T_3^2} \text{ cm}, \quad (17)$$

where  $L_{UV} = 10^{46} L_{UV,46}$  erg s<sup>-1</sup> is the luminosity of the accretion disc, and  $T = 10^3 T_3$  K is the effective temperature of dust. The dust provides radiation field with energy density which at  $r < r_{IR}$  is approximately constant and equal to

$$u_{IR} \simeq \xi_{IR} 4\sigma_{SB} T^4 / c \simeq 2.3 \times 10^{-3} (\xi_{IR}/0.3) T_3^4 \text{ erg s}^{-1}. \quad (18)$$

The model parameters are given in Table 2, and illustrated in Figures 1 – 3, which show time-averaged broad-band spectra computed using the model equations and assumptions given in §2. Specifically, we consider three cases: (1) a pure C(IR) model (**A**, shown in Fig. 1); (2) pure C(BEL) model (**B**, shown in Fig. 2); and (3) a combination of the two (**A+B**, shown in Fig. 3). In all three figures, a comparison of the four panels illustrates the dependence of the time averaged spectra on the low energy break in the injection function,  $\gamma_b$ .

To validate the models in greater detail, we also consider spectra obtained for the two well-studied objects. In Fig. 4 we present our model fits to the Jan-Feb 1996 outburst in 3C 279 (Wehrle

*et al.* 1998) and to the March 1995 outburst in PKS 0528+134 (Błażejowski *et al.* 1997; Kubo *et al.* 1998), using a combination of models **A** and **B**. The model parameters for those fits are presented in Table 2.

### 3.1. Spectra

Figures 1 – 3 clearly illustrate that the general features of spectra of  $\gamma$ -ray detected OVV quasars – in particular, the high ratio of Compton to synchrotron luminosities, and the comparative deficit of X-ray radiation – can be reproduced by both types of models, **A** (where C(IR) dominates) and **B** (where C(BEL) dominates). However, the details of the spectra are different. The models **A** yield X-ray spectra which are much smoother and closer to the observed ones than the spectra produced by models **B**. This results from the fact that in order to reproduce the observed spectra, in models **A**, the Lorentz factors of electrons/positrons  $\gamma_c$  (where the cooling break occurs) need to be larger than in models **B**, causing the X-ray portion of the SSC component to be harder in models **A** as compared to **B**.

Another important difference between these two models is in the high energy  $\gamma$ -ray spectral band. The spectral components due to C(IR) have a break at  $\sim 1$  GeV, whereas EGRET/*CGRO* observations show that blazar spectra extend at least up to 5 GeV. Therefore, the EGRET spectra can be reproduced only as a superposition of C(IR) and C(BEL) (see Fig. 3). This also provides an attractive explanation for  $\gamma$ -ray spectra being steeper than the X-ray spectra by more than the value predicted by cooling effect, *i.e.*,  $\Delta\alpha = 0.5$ . Examples of spectra of objects with  $\Delta\alpha > 0.5$ , often called “MeV blazars,” can be found in McNaron-Brown *et al.* (1995), Blom *et al.* (1995), and Malizia *et al.* (1999).

### 3.2. Low Energy Injection Break and Pair Content

Total number of relativistic electrons plus positrons injected in the shell during the flare is

$$N_e = \Delta t' \int_1^{\gamma_{max}} Q d\gamma \simeq \frac{r_0}{c\Gamma} \frac{K}{\gamma_b^{p-1}} \left( \ln \gamma_b + \frac{1}{p-1} \right), \quad (19)$$

where  $\Delta t' = \Delta r/c\Gamma = r_0/c\Gamma$  is the injection time interval. The number of protons enclosed in the shell is on the order of

$$N_p \simeq \dot{N}_p \Delta t_\lambda \simeq \frac{L_p}{m_p c^2 \Gamma} \frac{\lambda}{c}, \quad (20)$$

where  $L_p$  is the energy flux of cold protons in a jet and  $\lambda$  is the width of the shell as measured in the external frame. We note here that because the energy dissipated in a jet in our model results from collisions between inhomogeneities, one should not expect heating of protons to much larger average energies than mildly relativistic. Furthermore, this energy is quickly lost due to adiabatic expansion and/or converted back to the bulk energy. This is why jet energy flux is expected to be dominated by cold protons.



Combining Eqs. (19) and (20), we find

$$\frac{N_+}{N_p} \simeq \frac{N_e}{2N_p} \simeq \frac{m_p c^2 r_0}{2L_p} \frac{K}{\lambda} \frac{1}{\gamma_b^{p-1}} \left( \ln \gamma_b + \frac{1}{p-1} \right). \quad (21)$$

(We defined  $N_e$  as a sum of numbers of both relativistic electrons and positrons, and thus for  $N_+ >$  a few  $\times N_p$  the charge conservation gives  $N_e \sim 2N_+$ .) Assuming the kinetic luminosity of the jet to be  $L_j = 10^{47} L_{j,47} \sim 10^{47} \text{ erg s}^{-1}$  (see, e.g., Rawlings & Saunders 1991; Celotti & Fabian 1993) and noting that  $\lambda < r_0/\Gamma^2$  (see assumption about the shell width in §2), we obtain results presented in Table 3.

The pair content implied by our fits to the time averaged spectrum of the outburst in 3C 279 is  $n_+/n_p \simeq 4$ , and for the outburst in PKS 0528+134 —  $n_+/n_p \simeq 17$ . Note, however, that our fits are not unique, since such parameters as time scales of flares, energy densities of external radiation fields, and jet powers are not very well constrained by observations.

As we can see from Table 3, the pair content ranges from a few for  $\gamma_b \sim 100$  up to more than hundred for  $\gamma_b \sim 1$ . The recent detection of circular polarization in several compact radio sources (Wardle *et al.* 1998; Homan & Wardle 1999) and its interpretation in terms of the Faraday conversion process favor low values of  $\gamma_b$ , and therefore a large pair content. However, there are some objects with such hard X-ray spectra (Malizia *et al.* 1999; Fabian *et al.* 1998), that they can only be explained if  $\gamma_b \gg 1$ . But even in these cases, as long as  $\gamma_b < 100$ , at least some pair content is required. Such pairs can be produced via interaction of a cold proto-jet with radiation of the hot accretion disc corona (Sikora & Madejski 2000).

### 3.3. External Radiation Fields

As we can see from Table 1, in the models **A** and **A+B**,  $u_{IR} \sim 10^{-4} \text{ erg s}^{-1}$ , *i.e.* about 20 times less than energy density of radiation produced by silicate grains with its maximum temperature  $\simeq 1000 \text{ K}$ , and about 100 times less than energy density of radiation produced by graphite grains with its maximum temperature  $\simeq 1500 \text{ K}$ . This implies the value of  $u_{IR}$  to be lower than expected, in order to avoid overproduction of X-rays. In either model, the corresponding dust temperature is  $\sim 500 \text{ K}$ , *i.e.* 2-3 times lower than maximum, and the distance of dust from the central source is  $\sim 5\sqrt{L_{UV,46}} \text{ pc}$ . Alternatively, overproduction of X-rays by Comptonization of IR radiation can be avoided by postulating that the  $\gamma$ -ray luminosity peak is not defined by the value of the cooling break  $\gamma_c$  as assumed above, but rather, by the injection break  $\gamma_b$  (see Ghisellini *et al.* 1999; Mukherjee *et al.* 1999).

In the model **A+B**,  $u_{diff(BEL)} \simeq u_{diff(IR)} \simeq 10^{-4} \text{ erg cm}^{-3}$  (see Table 1), which is 30 times lower than the average in radio loud quasars. However, as recent reverberation campaigns show, broad emission lines have peak luminosities at distances  $\sim 3 \times 10^{17} \sqrt{L_{UV,46}} \text{ cm}$  (see review by Peterson 1993), and therefore the amount of the diffuse line radiation at distances where flares are produced ( $\sim r_0 \div 2r_0 \sim 10^{18} \text{ cm}$ ) is likely to be a small fraction of the total  $L_{BEL}$ . In case of models **B**,  $u_{diff(BEL)}$  is much closer to the observed values and there is no need for significant reduction of  $L_{BEL}$  at distances corresponding to  $r_0$ .

### 3.4. Bulk Compton Radiation

The models presented above don't take into account the so-called bulk-Compton process – the Comptonization of ambient diffuse radiation by cold electrons/positrons in a jet (Begelman & Sikora 1996; Sikora *et al.* 1997). This process should lead to the production of narrow bumps at energies  $\Gamma^2 h\nu_{ext}$ , *i.e.*,  $\sim 2 \times (\Gamma/15)^2$  keV and  $\sim 0.3 \times (\Gamma/15)^2$  keV for  $\nu_{ext} = \nu_{UV}$  and  $\nu_{ext} = \nu_{IR}$ , respectively. The largest contribution should come from very small distances, where the jet just starts to be relativistic and collimated. The absence of soft X-ray bumps in the observed spectra of OVV quasars (see, *e.g.*, Lawson & M<sup>c</sup>Hardy 1998) suggests that the region of jet formation is very extended, possibly reaching distances not very much smaller than those where most of blazar radiation is produced, or else, the number of pairs in a jet is very small (*cf.* Sikora *et al.* 1997). Noting that the number flux of cold pairs at  $r < r_0$  should at least be equal to the number flux of relativistic pairs accelerated at  $r \sim r_0$ , the latter condition corresponds to  $\gamma_b \gg 1$ .

### 3.5. Variability

Fig. 5 shows the time evolution of the broad-band spectrum presented in Fig. 3, binned in the time intervals  $\Delta t = t_0 \equiv r_0/2\Gamma^2 c$ . As one can see from those Figures, the flares decay at different rates in different spectral bands. Despite the transverse size of the source and related light travel effects, the dependence of energy losses on electron/positron energy is manifested very strongly, causing the synchrotron and Compton spectra above the luminosity peak to steepen with time. Additional steepening of the  $\gamma$ -ray spectrum is caused by the fact that C(BEL) drops faster with distance than C(IR). This is because the energy density of broad emission line light decreases with distance, while energy density of IR radiation is roughly constant. Such a steepening of  $\gamma$ -ray spectra is observationally confirmed both by direct observations of the slope changes during individual flares (Mücke *et al.* 1996; Mukherjee *et al.* 1996; Mattox *et al.* 1997), and statistically, by comparison of time averaged spectra as measured during different epochs (Pohl *et al.* 1997).

Steepening of the synchrotron spectrum is also consistent with observations, which show that the amplitude of variability increases with the increasing energy of the observing band. However, in many OVV quasars, the amplitude of the variability of the synchrotron component, even at the highest frequencies, is much smaller than amplitude of variability in  $\gamma$ -rays. A particularly clear example of such behavior is provided by the simultaneous multi-band observations of the Jan-Feb 1996 flare in 3C 279 (Wehrle *et al.* 1998). This can be explained by assuming that the synchrotron component is heavily contaminated by radiation produced at larger distances and/or by stationary shocks.

The situation at the keV energies is quite complex, but very interesting, as it provides important constraints on models. If the spectra measured in this range are entirely dominated by ERC components, then the drop of flux is predicted to be achromatic (with constant slope). This is because the low energy tails of ERC components are produced by electrons/positrons whose energy losses are dominated by adiabatic expansion. However, as suggested by Inoue & Takahara (1996) and Kubo *et al.* (1998) and confirmed by our models, the low energy X-rays are likely to

be dominated by the SSC component. Then the whole X-ray spectrum is a superposition of a softer SSC component and harder ERC component, which should result in a concave shape. Such spectra are in fact in a few cases observed directly, and are also implied by the fact that two-point slopes between the X-ray and  $\gamma$ -ray bands are harder than the X-ray spectra measured in the soft/mid X-ray bands alone (Comastri *et al.* 1997). As we can see from Fig. 5, such X-ray spectra – formed by a superposition of SSC and ERC components – harden as the source fades. This is caused by the SSC component, with luminosity which is proportional to the square of synchrotron luminosity, decaying faster than the low energy tail of ERC components. Hardening of X-ray spectra during the decay of the flare was in fact observed in some objects (see Ghisellini *et al.* 1999; Malizia *et al.* 1999). In most cases, however, the X-ray spectrum softens as the flare fades (Lawson, M<sup>c</sup>Hardy & Marscher 1999; Comastri *et al.* 1997). This discrepancy can be resolved by postulating that the X-ray spectra, particularly at the lowest energies, are contaminated by radiation produced either at larger distances (see, *e.g.*, Unwin *et al.* 1997), or in stationary shocks which may form if jet is reconfined and/or bent (see Komissarov & Falle 1997 and references therein). Furthermore, the light curves of outbursts can be further modified by a change of shell velocity (see, *e.g.*, Dermer & Chiang 1998), or by a change of direction of propagation. The latter case seems to be favored by VLBI observations, which often show strong curvature of jets in OVV quasars on parsec scales (Appl, Sol & Vicente 1996; Bower *et al.* 1997; Rantakyrö *et al.* 1998; Tingay, Murphy & Edwards 1998). Finally we emphasize that even very high amplitude flares are never isolated: observations show that they smoothly join with lower amplitude neighboring flares, forming with them longer lasting high states. In order to explain the continuously flaring high state light curves in terms of propagating shells of relativistic plasma, one must assume that number of shells per a distance range  $r_0 - 2r_0$  is on the order of  $N_{sh} \sim \Gamma^2$ . For this particular number, the number of shells contributing to the observed radiation at a given instant is  $N_{sh,obs} \sim N_{sh}/\Gamma^2 \sim 1$  (see Appendix in Sikora *et al.* 1997). For a much lower number of shells, the observer would see very isolated flares, while for much larger number of shells the resultant fluctuation (amplitude of the smaller flares superposed on the “high state”) would be smaller than is commonly observed.

#### 4. CONCLUSIONS

- Comptonization of infrared radiation produced by hot dust should be taken into account in all radiation models of blazars. Such radiation, likely to be present in quasar cores on parsec scales, is sufficiently dense to compete with broad emission line flux as the source of Compton cooling of relativistic electrons/positrons in parsec/sub-parsec jets;
- Both types of ERC models, either those where the  $\gamma$ -ray luminosity is dominated by C(IR) (models **A**) or those where the  $\gamma$ -ray luminosity is dominated by C(BEL) (models **B**), are able to reproduce all basic broadband spectral features of OVV quasars during their outbursts;
- If the blazar radiation is produced at distances larger than the distance at which the energy density of the broad emission line light peaks, the C(IR) component is expected to dominate over the C(BEL) component;

- The ERC models predict the general steepening of the  $\gamma$ -ray and synchrotron spectra with energy, in a qualitative agreement with observations. However, the lower observed variability amplitude of the synchrotron flux as compared with the  $\gamma$ -ray flux suggests a strong contamination of synchrotron radiation produced in the process of a flare by synchrotron radiation produced at larger distances or in stationary shocks;
- X-ray spectra in OVV quasars consist of SSC and ERC components, and the latter can be either C(IR) or C(BEL). Just as in the case of synchrotron radiation, additional contribution to the soft/mid energy X-rays is expected from quasi-steady component produced by distant and/or stationary shocks. This can explain why the amplitude of variability in the X-ray bands is smaller than in  $\gamma$ -rays;
- The ERC models of  $\gamma$ -ray production predict the pair content of the jet plasma,  $n_+/n_p$ , to be in the range from a few  $\times L_{j,47}$  for  $\gamma_b \sim 100$  up to hundred  $\times L_{j,47}$  for  $\gamma_b \sim 1$ . Low values of  $\gamma_b$  (and therefore a large  $e^+/e^-$  pair content) are favored by observations of circular polarization, assuming its interpretation in terms of the Faraday conversion process is correct.

The project was partially supported by Polish KBN grant 2P03D 00415, ITP/NSF grant PHY94-07194, NASA grants NAG-6337 and NASA observing/ADP grants to the University of Maryland and USRA.

## REFERENCES

- Appl, S., Sol, H., & Vicente, L. 1996, A&A, 310, 419
- Begelman, M.C., & Sikora, M. 1987, ApJ, 322, 650
- Blandford, R.D., & Levinson, A. 1995, ApJ, 441, 79
- Blom, J.J., *et al.* 1995, A&A, 295, 330
- Błażejowski, M., *et al.* 1997, in “Relativistic Jets in AGNs,” (Proc. of Conf. in Kraków, 27-30 May, 1997), eds M. Ostrowski, M. Sikora, G. Madejski, & M.C. Begelman, 233
- Bower, G.C., Backer, D.C., Wright, M., Forster, J.R., Aller, H.D., & Aller, M.F. 1997, ApJ, 484, 118
- Brown, L.M.J., Robson, E.I., Gear, W.K., Smith, M.G. 1989, ApJ, 340, 150
- Cao, X., & Jiang, D.R. 1999, MNRAS, 307, 802
- Celotti, A., & Fabian, A.C. 1993, MNRAS, 264, 2280
- Celotti, A., Padovani, P., & Ghisellini, G. 1997, MNRAS, 286, 415
- Chiang, J., & Dermer, C.D. 1999, ApJ, 512, 699

- Comastri, A., Fossati, G., Ghisellini, G., & Molendi, S. 1997, *ApJ*, 480, 534
- Coppi, P.S., & Aharonian, F.A. 1999, *ApJ*, 521, L33
- Dermer, C.D. 1995, *ApJ*, 446, L63
- Dermer, C.D., & Chiang, J. 1998, *New Astronomy*, 3, 157
- Dermer, C.D. & Schlickeiser, R. 1993, *ApJ*, 416, 458
- de Vries, W.H., O’Dea, C.P., Baum, S.A., Perlman, E., Lehnert, M.D., & Barthel, P.D. 1998, *ApJ*, 503, 156
- Dondi, L. & Ghisellini, G. 1995, *MNRAS*, 273, 583
- Edelson, R. 1992, *ApJ*, 401, 516
- Fabian, A.C., Iwasawa, K., Celotti, A., Brandt, W.N., McMahon, R.G., & Hook, I.M. 1998, *MNRAS*, 295, L25
- Fossati, G., Maraschi, L., Celotti, A., Comastri, A., & Ghisellini, G. 1998, *MNRAS*, 299, 433
- Ghisellini, G., Celotti, A., Fossati, G., Maraschi, L., & Comastri, A. 1998, *MNRAS*, 301, 451
- Ghisellini, G., *et al.* 1999, *A&A*, 348, 63
- Hartman, R.C., *et al.* 1996, *ApJ*, 461, 698
- Homan, D.C., & Wardle, J.F.C. 1999, *AJ*, 118, 1942
- Hoshino, M., Arons, J., Gallant, Y.A., & Langdon, A.B. 1992, *ApJ*, 390, 454
- Inoue, S., & Takahara, F. 1996, *ApJ*, 463, 555
- Kirk, J.G., Rieger, F.M., & Mastichiadis, A. 1998, *A&A*, 333, 452
- Komissarov, S.S., & Falle, S.A.E.G. 1997, *MNRAS*, 288, 833
- Kubo, H., *et al.* 1998, *ApJ*, 504, 693
- Kusunose, M., Takahara, F., & Li, H. 2000, *astro-ph/0002137*
- Lawson, A.J., & McHardy, I.M. 1998, *MNRAS*, 300, 1023
- Lawson, A.J., McHardy, I.M., & Marscher, A.P. 1999, *MNRAS*, 306, 247
- Levinson, A. 1996, *MNRAS*, 278, 1018
- Madejski, G.M., Sikora, M., Jaffe, T., Błażejowski, M., Jahoda, K., & Moderski, R. 1999, *ApJ*, 521, 145

- Malizia, A., Bassani, L., Dean, A.J., McCollough, M., Stephen, J.B., Zhang, S.N., & Paciesas, W.S. 1999, astro-ph/9910484
- Mastichiadis, A. & Kirk, J.G. 1997, A&A, 320, 19
- Mattox, J.R., Wagner, S.J., Malkan, M., McGlynn, T.A., Schachter, J.F., Grove, J.E., Johnson, W.N., & Kurfess, J.D. 1997, ApJ, 476, 692
- McClements, K.G., Dendy, R.O., Bingham, R., Kirk, J.G., & Drury, L., O’C. 1997, MNRAS, 291, 241
- McHardy, I., Lawson, A., Newsam, A., Marscher, A., Robson, I., & Stevens, J. 1999, MNRAS, 310, 571
- McNaron-Brown, K., *et al.* 1995, ApJ, 451, 575
- Michelson, P.F., *et al.* 1994, in AIP Conf. Proc. No. 304, Proc. 2nd Compton Symp., ed. C.E. Fichtel, N. Gehrels, & J.P. Norris (New York: AIP), 602
- Moderski, R., Sikora, M., & Bulik, T. 2000, ApJ, 529, 151
- Mukherjee, R., *et al.* 1996, ApJ, 470, 831
- Mukherjee, R., *et al.* 1999, ApJ, 527, 132
- Mücke, A., Pohl, M., Kanbach, G., *et al.* 1996, in “Extragalactic radio sources”, IAU Symposium 175, Kluwer, Dordrecht, 285
- Peterson, B.M. 1993, PASP, 105, 247
- Pohl, M., Hartman, R.C., Jones, B.B., & Sreekumar, P. 1997, A&A, 326, 51
- Rantakyö, F.T., *et al.* 1998, A&A, 131, 451
- Rawlings, S., & Saunders, R. 1991, Nature, 349, 138
- Rees, M.J., & Mészáros, P. 1994, ApJ, 430, L93
- Rybicki, G.B., & Lightman, A.P. 1979, Radiative Processes in Astrophysics, (New York: John Wiley & Sons, Inc.)
- Sambruna, R.M. 1997, ApJ, 487, 536
- Sanders, D.B., *et al.* 1989, ApJ, 347, 29
- Sikora, M. 1997, AIP Conference Proceedings (4th Compton Symposium), 410, 494
- Sikora, M., Begelman, M.C., & Rees, M.J. 1994, ApJ, 421, 153 [SBR94]

- Sikora, M., & Madejski, G. 2000, ApJ, 534, 109
- Sikora, M., Madejski, G., Moderski, R., & Poutanen, J. 1997, ApJ, 484, 108
- Tingay, S.J., Murphy, D.W., & Edwards, P.G. 1998, ApJ, 500, 673
- Ulrich, M.-H., Maraschi, L., & Urry, C.M. 1997, ARA&A, 35, 445
- Unwin, S.C., Wehrle, A.E., Lobanov, A.P., Zensus, J.A., Madejski, G.M., Aller, M.F., & Aller, H.D. 1997, ApJ, 480, 596
- von Montigny, C., *et al.* 1995, ApJ, 440, 525
- Wardle, J.F.C., Homan, D.C., Ojha, R., & Roberts, D. 1998, Nature, 395, 457
- Wagner, S.J., *et al.* 1995a, A&A, 298, 688
- Wagner, S.J., *et al.* 1995b, ApJ, 454, L97
- Wehrle, A.E. *et al.* 1998, ApJ, 497, 178

## A. RELATIVISTIC TRANSFORMATION OF OBSERVED LUMINOSITY

### (1) *The case of a point source of radiation*

Observed monochromatic luminosity of a point source at the moment  $t$  is

$$\delta L_\nu[t] \equiv 4\pi \frac{dP_\nu}{d\Omega}[t] = 4\pi \mathcal{D}^3 \frac{dP'_{\nu'}}{d\Omega'}[t'] \equiv \mathcal{D}^3 \delta L'_{\nu'}[r; \vec{n}'_{obs}], \quad (\text{A1})$$

(Rybicki & Lightman 1979), where

$$r = \frac{c\beta t}{1 - \beta \cos \theta}, \quad (\text{A2})$$

$$\mathcal{D} = \frac{1}{\Gamma(1 - \beta \cos \theta)} \equiv \Gamma(1 + \beta \cos \theta'), \quad (\text{A3})$$

$\nu' = \nu/\mathcal{D}$ , and  $\theta$  is the angle between the direction of the source motion and the direction to the observer,  $\vec{n}'_{obs}$ .

### (2) *The case of an extended source of radiation*

Since we are only interested in the optically thin radiation, the observed luminosity of an extended source can be computed by summing contribution from its small pieces, treated as point sources. Of course, because of light travel effects, for pieces moving along different  $\theta$ 's, contribution

must be taken from different distances (see Eq. A2). Using approximation of infinitely thin shell ( $\lambda \ll r_0/\Gamma^2$ ), we divide the source into  $\delta\Omega_j = \Omega_j/N$  pieces, where N must be enough large to allow treat individual pieces as point sources (*i.e.*, with negligible light travel effects). The observed luminosity is then given by

$$(\nu L_\nu)[t] = \Sigma_N (\nu \delta L_\nu)[\theta; t] = \Sigma_N \mathcal{D}^4(\nu' \delta L'_{\nu'})[r; \vec{n}'_{obs}]. \quad (\text{A4})$$

For uniform shells, one can introduce the formal quantity, “intrinsic luminosity”  $L'_\nu[\theta; t] = \delta L'_\nu[\theta; t] \times N = \delta L'_\nu[\theta; t] \times (\Omega_j/\delta\Omega_j)$ , and with this and  $N \rightarrow \infty$ , Eq. (A4) can be converted into Eq. (8).



**FIGURE CAPTIONS**

Fig. 1.— Time averaged model spectra of blazars for four values of  $\gamma_b$ . The dotted line marks the typical slope of the X-ray spectra observed in OVV-type blazars ( $\alpha = 0.6$ ); the dashed lines enclose the 1–30 keV X-ray band. In each panel we show three spectral components: synchrotron (SYN), synchrotron-self-Compton (SSC) and Comptonization of near-IR dust radiation [C(IR)]. (Model A). (For the model parameters, see Table 1).

Fig. 2.— Same as Fig. 1, but C(IR) is replaced with C(BEL) (Model B).

Fig. 3.— Same as Fig. 1, where both C(IR) and C(BEL) are included (Model A+B).

Fig. 4.— Left panel: model fit to the outburst spectrum observed in PKS 0528+134 (Model A+B). The X-ray spectra (ASCA) and  $\gamma$ -rays (EGRET) are simultaneous (McNaron-Brown *et al.* 1995; Kubo *et al.* 1998). Radio and optical data are nonsimultaneous and are taken from the archive sources (see Błażejowski *et al.* 1997 for details and references therein). Right panel: model fit to the outburst spectrum observed in 3C 279. Radio, optical, X-ray and  $\gamma$ -ray data are simultaneous (Wehrle *et al.* 1998) (Model A+B).

Fig. 5.— Binned spectra in the time intervals  $\Delta t = r_0/2\Gamma^2c$  (Model A+B).

Table 1. Parameters used in models

MODEL	$\Gamma$	$r_0[cm]$	$B_0[G]$	$K[\frac{1}{s}]$	$\gamma_b$	$\gamma_{max}$	p	$U_{BEL,0}[\frac{erg}{cm^3}]$	$U_{IR}[\frac{erg}{cm^3}]$
A	15	$7.0 \times 10^{17}$	0.43	$6.8 \times 10^{49}$	1 - 100	$6.0 \times 10^3$	2.2	0.0	$10^{-4}$
B	15	$6.0 \times 10^{17}$	1.34	$6.9 \times 10^{49}$	1 - 100	$1.0 \times 10^4$	2.2	$2.3 \times 10^{-3}$	0.0
A+B	15	$7.0 \times 10^{17}$	0.43	$8.9 \times 10^{49}$	1 - 100	$6.0 \times 10^3$	2.2	$10^{-4}$	$10^{-4}$

Table 2. Parameters used in modeling 3C 279 and PKS 0528+134

OBJECT	$\Gamma$	$r_0[cm]$	$B_0[G]$	$K[\frac{1}{s}]$	$\gamma_b$	$\gamma_{max}$	p	$U_{BEL,0}[\frac{erg}{cm^3}]$	$U_{IR}[\frac{erg}{cm^3}]$
3C 279	20	$7.0 \times 10^{17}$	0.81	$2.8 \times 10^{50}$	150	$6.5 \times 10^3$	2.4	$0.6 \times 10^{-3}$	$0.2 \times 10^{-3}$
PKS 0528+134	15	$7.0 \times 10^{17}$	1.7	$1.2 \times 10^{50}$	25	$4.7 \times 10^3$	2.2	$2.1 \times 10^{-3}$	$4.7 \times 10^{-4}$

Table 3.  $(n_+/n_p)_{min}$  ratios.

$\gamma_b$	1	5	20	100
A	96	40	12	2
B	97	41	12	2

FIG. 1.

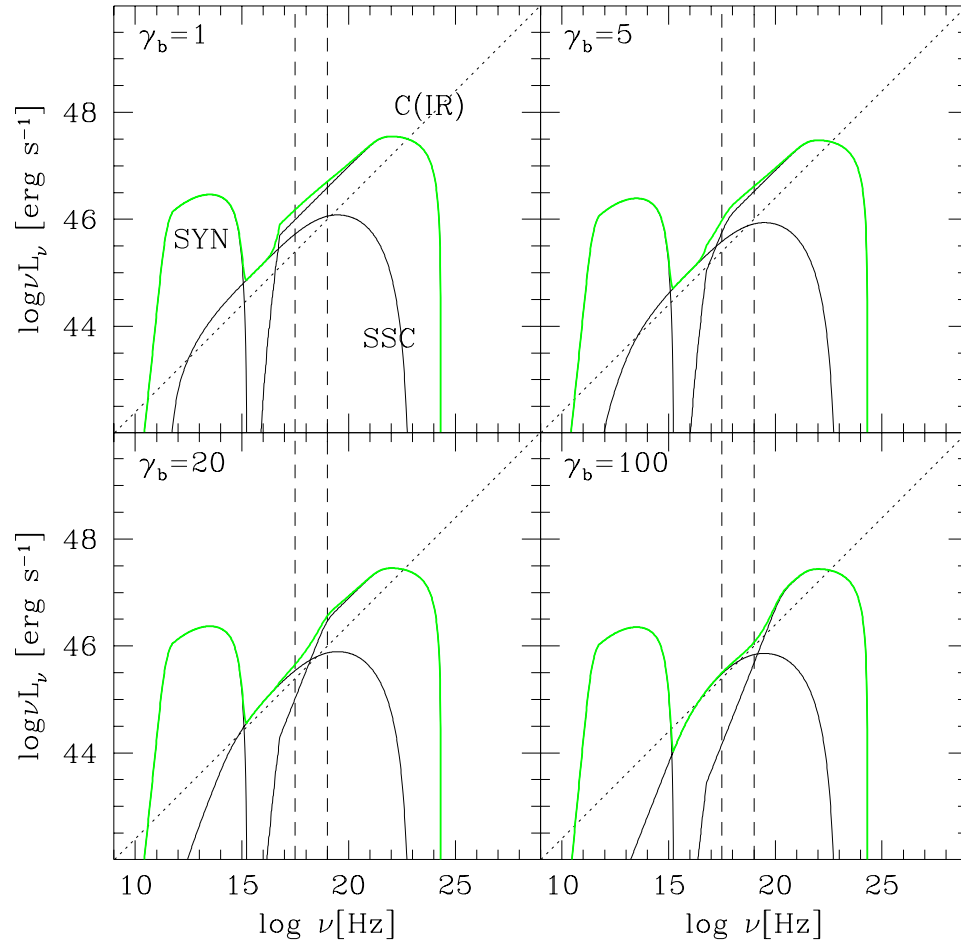


FIG.2.

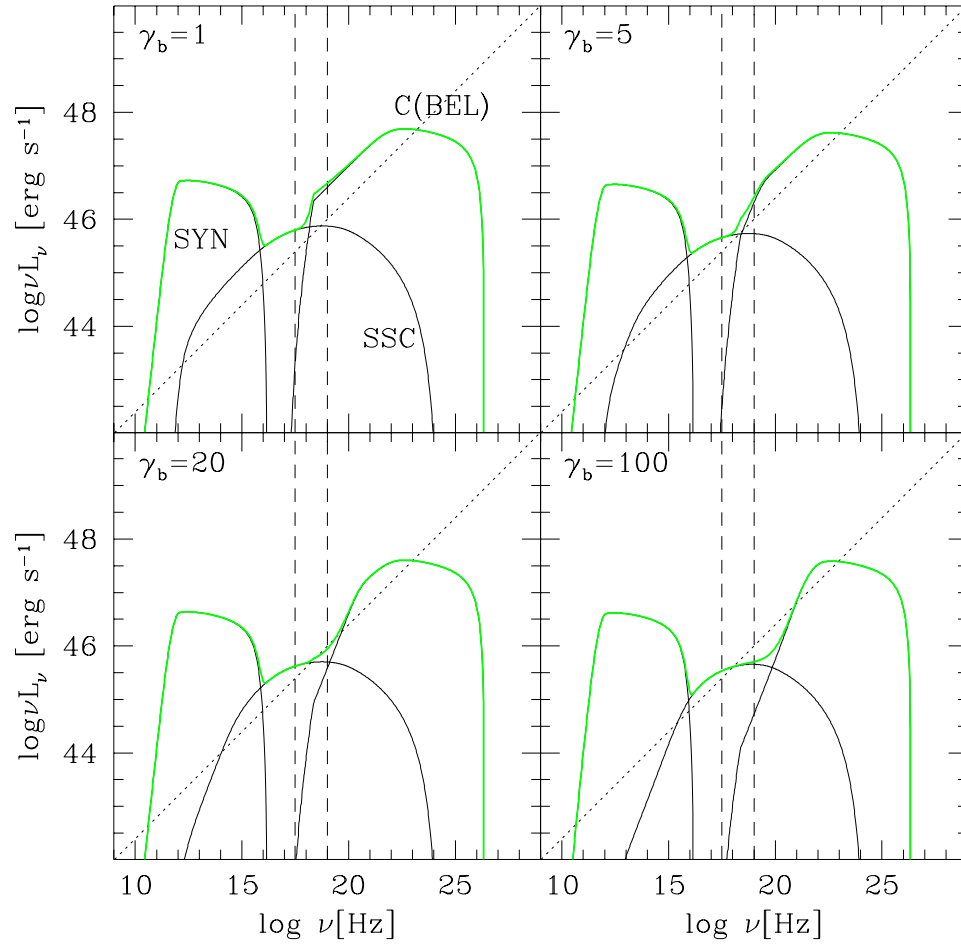


FIG.3.

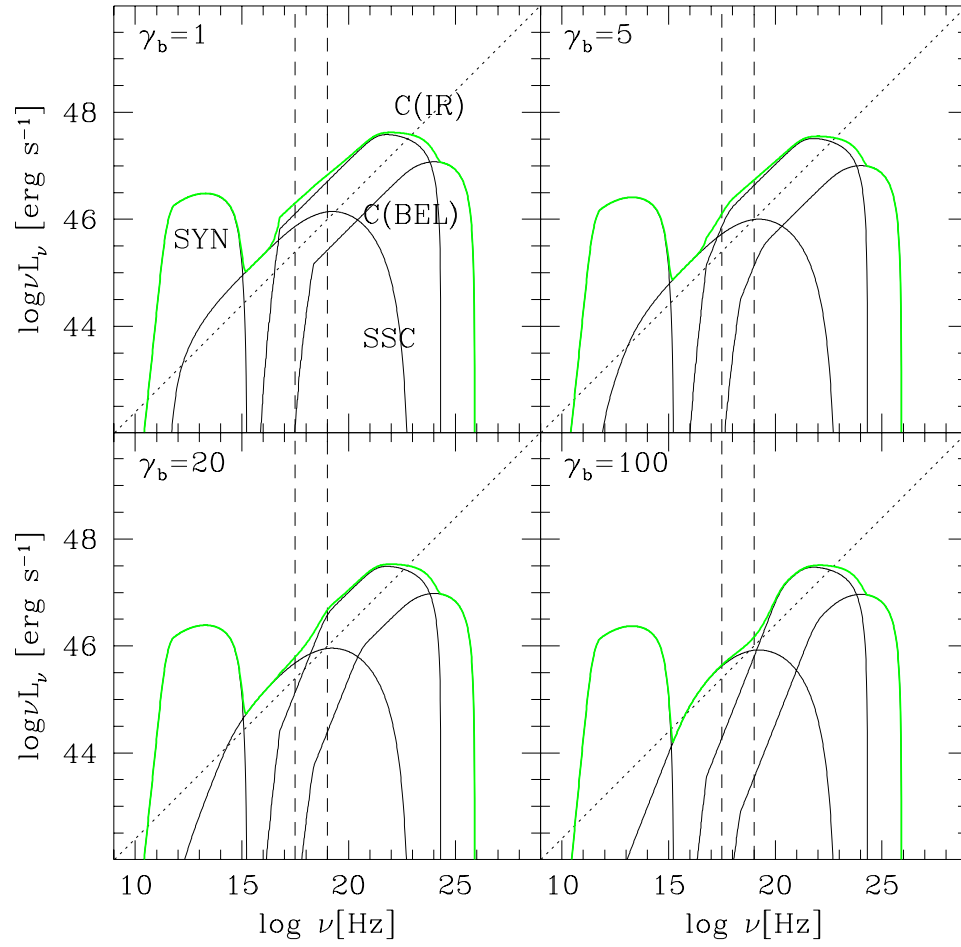


FIG.4.

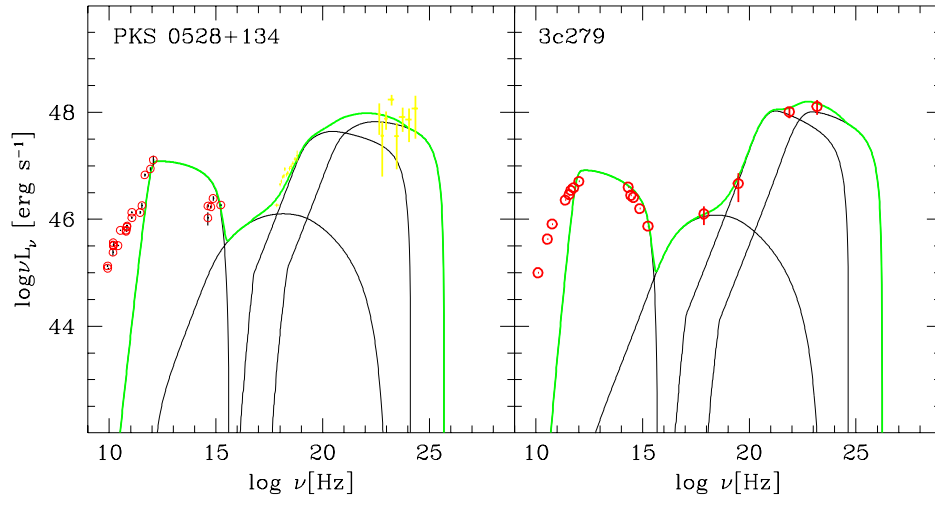


FIG.5.

